Weierstraß-Institut
für Angewandte Analysis und Stochastik
Leibniz-Institut im Forschungsverbund Berlin e. V.

Preprint ISSN 2198-5855

Dynamics of an inhomogeneously broadened passively mode-locked laser

Alexander Pimenov, Andrei G. Vladimirov

submitted: November 15, 2018

Weierstrass Institute
Mohrenstr. 39
10117 Berlin
Germany
E-Mail: alexander.pimenov@wias-berlin.de
andrei.vladimirov@wias-berlin.de

No. 2551
Berlin 2018

2010 *Physics and Astronomy Classification Scheme.* 42.60.Fc, 42.55.Px, 42.60.Gd, 05.45.-a, 02.30.Ks.

Key words and phrases. Laser dynamics, passive mode-locking, inhomogeneous broadening, Q-switching, traveling wave model, delay differential equations.

A. P. and A. G. V. acknowledge the support of SFB 787 of the DFG.

Edited by
Weierstraß-Institut für Angewandte Analysis und Stochastik (WIAS)
Leibniz-Institut im Forschungsverbund Berlin e. V.
Mohrenstraße 39
10117 Berlin
Germany

Fax: +49 30 20372-303
E-Mail: preprint@wias-berlin.de
World Wide Web: http://www.wias-berlin.de/

Dynamics of an inhomogeneously broadened passively mode-locked laser

Alexander Pimenov, Andrei G. Vladimirov

Abstract

We study theoretically the effect of inhomogeneous broadening of the gain and absorption lines on the dynamics of a passively mode-locked laser. We demonstrate numerically using travelling wave equations the formation of a Lamb-dip instability and suppression of Q-switching in a laser with large inhomogeneous broadening. We derive simplified delay-differential equation model for a mode-locked laser with inhomogeneously broadened gain and absorption lines and perform numerical bifurcation analysis of this model.

1 Introduction

Passively mode-locked lasers generate short optical pulses used in numerous scientific, technological, and industrial applications. In particular, monolithic semiconductor lasers are compact sources of picosecond and subpicosecond pulses with high repetition rates suitable for application in telecommunication networks [1]. Recent experimental and theoretical investigations have demonstrated that new generations of quantum dot and quantum dash semiconductor lasers have important advantages over conventional quantum-well semiconductor devices: low threshold current, low pulse chirp, reduced temperature sensitivity, high stability to noise and external feedback, etc [2, 3]. One of the important features of these lasers that plays a major role in determining various laser characteristics is the inhomogeneous broadening of the gain spectrum due to nonuniformity of the ensemble of quantum dots with respect to their size, shape, and composition [2]. In particular, it was demonstrated that in quantum dot lasers under the bias conditions the inhomogeneous broadening width at half-maximum (from 21 meV to 50 meV) is larger than homogeneous broadening width (19 meV) [4].

The effect of inhomogeneous broadening on single-mode [5–11], multi-longitudinal [12–18] and multi-transverse [19, 20] mode laser instabilities have been a subject of intense studies during past decades. In particular, it was shown that inhomogeneous broadening can reduce the so-called second laser threshold as well as the threshold of the multimode Risken-Nummendal-Graham-Haken instability leading to a self-pulsing behavior. This is in agreement with common knowledge that inhomogeneous broadening of the gain line facilitates multimode operation. On the other hand, elementary considerations suggesting that ultrashort-pulse formation should be more easily achievable in inhomogeneously broadened lasers than in corresponding homogeneous systems, were shown to be in contradiction with the experimental data [21].

While the dynamics of inhomogeneously broadened CW lasers has been already extensively investigated, the influence of inhomogeneous broadening on the characteristics of passively mode-locked lasers still remains largely unexplored theoretically. In order to fill this gap in this work we study numerically the dynamics of a passively mode-locked laser with inhomogeneously broadened gain and absorber media. We consider traveling wave equations (TWEs) for the electric field envelopes of the counter-propagating waves coupled to the equations for polarizations and population differences of

DOI 10.20347/WIAS.PREPRINT.2551 Berlin 2018

the two-level atoms emitting at different central frequencies through the integral over these frequencies [20]. We integrate the resulting integro-differential equations numerically with the help of an efficient spectral method with Hermite-Gaussian functions taken as the basis functions. To this end, similarly to Graham and Cho [7], we derive an infinite chain of equations for the macroscopic variables, truncate this chain, and solve the truncated equations numerically. Unlike the analytical approach of Graham and Cho [7], our numerical techniques allows to perform the truncation at much higher orders and, therefore, to achieve better precision. Basing on our simulations we demonstrate that for moderate values of the inhomogeneous broadening linewidth the mode-locking characteristics can be improved due to suppression of the Q-switching instability. On the other hand, large inhomogeneous broadening linewidths lead eventually to a degradation of the mode-locking regime.

Finally, by assuming unidirectional propagation of the electrical field in the ring cavity and using the approach proposed in [22–24], we derive a simplified delay-differential equation (DDE) model of a mode-locked laser with inhomogeneously broadened gain and absorption lines. This model provides a good qualitative description of the nonlinear dynamical regimes in a laser by taking into consideration zero and first moments of medium polarization [7, 10]. We perform numerical bifurcation analysis of the DDE model and demonstrate qualitative agreement with the TWE model. We show that the Lamb-dip instability of the mode-locking regime develops when the inhomogeneous broadening width of the gain line exceeds a certain threshold and the suppression of Q-switching instability of the fundamental mode-locked regime can be achieved at sufficiently large inhomogeneous broadening linewidth of the saturable absorber.

2 Model equations

2.1 Travelling wave model

We consider non-dimensional form of the TWE model describing space-time evolution of the amplitudes $E^{\pm}(t,z)$ of the two counter-propagating waves, corresponding polarizations $P^{\pm}=P^{\pm}\omega,t,z)$, and population difference $N=N(\bar{\omega},t,z)$ of the two-level inhomogeneously broadened medium. These equations are obtained from the two-level semiclassical Maxwell-Bloch equations under standard mean-field, effective-index, and slowly varying envelope approximations [20].

$$\frac{\partial E^{\pm}}{\partial t}\pm\frac{\partial E^{\pm}}{\partial z}=-\frac{\beta}{2}E^{\pm}+\int_{-\infty}^{\infty}P^{\pm}\bar{f}(\bar{\omega})d\bar{\omega}, \tag{1}$$

$$\frac{\partial P^{\pm}}{\partial t}=(-\Gamma+i\bar{\omega})P^{\pm}+\frac{g}{2}NE^{\pm}, \tag{2}$$

$$\frac{\partial N}{\partial t}=n_0-\gamma_N N-\mathrm{Re}(P^{+}E^{+*}+P^{-}E^{-*}). \tag{3}$$

Here β describes internal linear losses in the intracavity medium, g is the differential gain parameter, Γ and γ_N are the transverse and longitudinal relaxation rates, respectively, and $n_0=n_0(z)$ is the linear gain/loss parameter. The normalized spectral distribution $\bar{f}(\bar{\omega})$ is represented by the Gaussian profile

$$\bar{f}(\bar{\omega})=\frac{1}{\sigma\sqrt{2\pi}}\exp\left(-\frac{(\bar{\omega}-\omega_0)^2}{2\sigma^2}\right), \tag{4}$$

where σ is the width of inhomogeneous broadening at half-maximum, ω_0 is the detuning between the central frequency of the Gaussian distribution (4) and the frequency of one of the cavity modes, which serves as the reference frequency.

2.2 Spectral method

For numerical solution of Eqs. (1)-(4) we use a "spectral" (Galerkin) method. First, we choose Hermite-Gaussian functions

$$\phi_m(\omega) = (m!2^m\sqrt{\pi})^{-1/2}e^{-\omega^2/2}H_m(\omega), \tag{5}$$

where $H_m(\omega)$ is the Hermite polynomial of the order m, as a complete orthonormal basis for the space $L^2(\mathbb{C})$ with the inner product defined by

$$\langle u, v\rangle = \int_{-\infty}^{\infty} uv^* d\omega \tag{6}$$

After the coordinate change

$$\omega = \frac{\bar{\omega} - \omega_0}{\sqrt{2}\sigma}, \tag{7}$$

the spectral distribution $\bar{f}(\bar{\omega})$ given by Eq. (4) transforms into $f(\omega) = \phi_0^2$ with $\phi_0 = \pi^{-1/4}e^{-\omega^2/2}$. Therefore, we can rewrite (1) in the form

$$\frac{\partial E^{\pm}}{\partial t} \pm \frac{\partial E^{\pm}}{\partial z} = P_0^{\pm} - \frac{\beta}{2}E^{\pm} \tag{8}$$

with $P_0^{\pm} = \langle P^{\pm}(\omega, t, z)\phi_0(\omega), \phi_0(\omega)\rangle$. Then multiplying Eqs. (2) and (3) with ϕ_0, projecting them onto ϕ_m, taking into account the coordinate change (7), and using the recurrent relations for Hermite polynomials we obtain an infinite hierarchy of equations for the moments $P_m^{\pm}(t, z) = \langle P^{\pm}(\omega, t, z)\phi_0(\omega), \phi_m(\omega)\rangle$ and $N_m(t, z) = \langle N(\omega, t, z)\phi_0(\omega), \phi_m(\omega)\rangle$:

$$\frac{\partial P_m^{\pm}}{\partial t} = (-\Gamma + i\omega_0)P_m^{\pm} + i\sigma(\sqrt{m}P_{m-1}^{\pm} + \sqrt{m+1}P_{m+1}^{\pm}) + \frac{g}{2}N_m E^{\pm}, \tag{9}$$

$$\frac{\partial N_m}{\partial \tau} = n_{0m} - \gamma_N N_m - \mathrm{Re}(E^+P_m^{+*} + E^-P_m^{-*}), \tag{10}$$

where $P_{-1}^{\pm} \equiv 0$.

In terms of original problem (1)-(3) the first two moments of polarization and population inversion have the form $P_j^{\pm} = \int_{-\infty}^{\infty} \omega^j P^{\pm} f(\omega)d\omega$ and $N_j = \int_{-\infty}^{\infty} \omega^j N f(\omega)d\omega$ with $j = 0, 1$ and $f(\omega) = \phi_0(\omega)^2$. They are equivalent to the zeroth- and the first-order moments of polarisation $P^{\pm}$ and carrier density N introduced by Graham and Cho [7]. Since $n_{0m} = 0$ for all $m > 0$, only the zeroth-order moment of the population difference is pumped directly, while other moments are excited via a purely imaginary constant in Eq (9).

When solving numerically equations (8)-(10) we choose some finite M and truncate them by setting $P_{M+1}^{\pm} = 0$. Though there is not much mathematical theory beyond partial integro-differential equations (1)-(3), the finite-dimensional hyperbolic system of PDEs (8)-(10) is well-posed [25]. Using energy estimates for the system (8)-(10) given in Appendix B one can show that the moments decrease with the number $m > 0$, i.e. $|P_m^{\pm}|, |N_m| \le c_k m^{-k}$ with any integer $k > 0$ and some constants $c_k > 0$ that do not depend on m and M. Therefore, solution of Eqs. (8)-(10) truncated at sufficiently large $m = M$ must be close to that of the same equations truncated at $m = M_1 > M$. Or, in other words, this solution must be close to the solution of the non-truncated equations. It is evident from the equation (9) that the speed of decrease of the moments with m depends strongly on the value of σ. In this sense, the chosen approach provides good quantitative approximation with the truncation order $M = 1$ for the case of small σ.

Truncating Eqs. (8)-(10) at $M = 1$ and eliminating adiabatically $P_1^{\pm}$ we obtain the following equation for $P_0^{\pm}$:

$$\frac{\partial P_0^{\pm}}{\partial t} = -\left(\Gamma + \frac{\sigma^2}{\Gamma}\right) P_0^{\pm} + \frac{\Gamma}{2} N_0 E^{\pm}. \tag{11}$$

Hence, we conclude that for small enough σ the basic effect of inhomogeneous broadening is to increase the homogeneous broadening width Γ by approximately σ^2/Γ .

3 Delay-differential equation model

In this section, we introduce a DDE system to describe an inhomogeneously broadened mode-locked semiconductor laser. First, we derive in Appendix a DDE model taking into account the polarization dynamics in two-level active medium. This model can be easily generalized to take into account inhomogeneous broadening. The resulting system of distributed DDEs reads

$$\gamma^{-1}\frac{dA}{dt} + (1 - i\omega_0/\gamma)A = \sqrt{\kappa}\,[A(t-\tau) + \langle P_q(\omega_q), f_q(\omega_q)\rangle + \langle P_g(\omega_g), f_g(\omega_g)\rangle]\,, \tag{12}$$

$$\frac{dP_q}{dt} = (-\Gamma_q + i\omega_q)P_q + \Gamma_q(e^{-Q/2} - 1)A(t-\tau), \tag{13}$$

$$\frac{dP_g}{dt} = -(\Gamma_g - i\omega_g)P_g + \Gamma_g(e^{G/2} - 1)[A(t-\tau) + P_q], \tag{14}$$

$$\frac{dQ}{dt} = q_0 - \gamma_q Q + s|A(t-\tau) + P_q|^2 - s|A(t-\tau)|^2, \tag{15}$$

$$\frac{dG}{dt} = g_0 - \gamma_g G + |A(t-\tau) + P_q|^2 - |A(t-\tau) + P_g + P_q|^2, \tag{16}$$

where $A(t)$ is the complex electric field amplitude, $G(t)$ and $Q(t)$ represent saturable gain and absorption introduced by the corresponding laser media. Parameters g_0 and q_0 describe unsaturated gain and absorption, respectively, $\kappa < 1$ is the cavity round trip attenuation factor, s is the ratio of the saturation intensities in the gain and absorber media, $\tau = 2l$ is the cavity round-trip time. $\Gamma_{g,q}$ and $\gamma_{g,q}$ are, respectively, transverse and longitudinal relaxation rates in the gain and absorber media, and $\omega_{g,q}$ describe the shift of the central frequencies of the gain and absorption lines from the reference frequency. Here the index g (q) corresponds to the gain (absorber) medium. The main role of the linear filtering term $\gamma^{-1}dA\,(t)\,/(dt)$ is to regularize the system by converting delay algebraic-differential equations into DDEs. The parameters γ and ω_0 represent width and the central frequency of the linear filter. In order minimize the effect of the linear filter on the system's dynamics in numerical simulations we choose $\gamma \gg \Gamma_g$. Note that in the case of homogeneous broadening with $\omega_{g,q} = 0$ Eqs (12)-(16) can be transformed into the standard DDE mode-locking model [22–24] by means of adiabatic elimination of polarizations $P_{g,q}$.

We further assume that the effect of inhomogeneous broadening on the dynamics of population difference is much weaker than its effect on the polarization dynamics [7, 10]. Then, implying that g_0 and q_0 are frequency independent, we assume $G(t)$ and $Q(t)$ to be frequency independent as well and

apply the spectral method to obtain the following truncated system

$$\frac{dA}{dt} + (\gamma - i\omega_0)A = \sqrt{\kappa}\gamma\big[A\,(t-\tau) + P_{0q} + P_{0g}\big], \tag{17}$$

$$\frac{dP_{0q}}{dt} = (-\Gamma_q + i\omega_{0q})P_{0q} + i\sigma_q P_{1q} + \Gamma_q(e^{-Q/2} - 1)A(t-\tau), \tag{18}$$

$$\frac{dP_{1q}}{dt} = -\left(\Gamma_q + \sqrt{2}p_{2q}\sigma_q + i\omega_{0q}\right)P_{1q} + i\sigma_q P_{0q}, \tag{19}$$

$$\frac{dP_{0g}}{dt} = (-\Gamma_g + i\omega_{0g})P_{0g} + i\sigma_g P_{1g} + \Gamma_g(e^{G/2} - 1)\left[A(t-\tau) + P_{0q}\right], \tag{20}$$

$$\frac{dP_{1g}}{dt} = \left(-\Gamma_g - \sqrt{2}p_{2g}\sigma_g + i\omega_{0g}\right)P_{1g} + i\sigma_g P_{0g}. \tag{21}$$

$$\frac{dQ}{dt} = q_0 - \gamma_q Q + s|A(t-\tau) + P_{0q}|^2 - s|A(t-\tau)|^2, \tag{22}$$

$$\frac{dG}{dt} = g_0 - \gamma_g G - |A(t-\tau) + P_{0g} + P_{0q}|^2 + |A(t-\tau) + P_{0q}|^2, \tag{23}$$

where $P_{0,1}$ represent the zeroth- and first-order moments of polarization, while all other moments satisfying differential equations

$$\frac{dP_m}{dt} = (-\Gamma + i\omega_0)P_m + i\sigma(\sqrt{m}P_{m-1} + \sqrt{m+1}P_{m+1}), \tag{24}$$

are eliminated adiabatically. The coefficients p_2 in Eqs. (19) and (21) can be approximated by setting $P_{M+1} = 0$ with M large enough. Then from Eq. (24) we get $P_M = ip_M P_{M-1}$ with $p_M = \sqrt{M}\sigma/\left(\Gamma - i\omega_0\right)$ and $P_m = ip_m P_{m-1}$ for all $2 < m < M-1$ with recursive relationship

$$p_m = \frac{\sqrt{m}\sigma}{\Gamma + i\omega_0 + \sqrt{m+1}\sigma p_{m+1}}.$$

Therefore, for $\omega_0 = 0$ we can see that $p_2 > 0$ and the main effect of the higher moments of polarization is that they increase the relaxation rate of the first moment of polarization for higher values of σ so that it becomes larger than relaxation rate of the zeroth-order moment of polarization.

In the particular case when inhomogeneous broadening is present only in the gain medium we set $\sigma_q = 0$ in the absorber medium. Furthermore in this case without the loss of generality we can assume that $\omega_{0q} = 0$. Then eliminating adiabatically the variable P_{0q} from Eq. (18) we obtain the relations $P_{0q} = (e^{-Q(t)/2} - 1)A(t-\tau)$ and $P_{1q} = 0$, which lead to the following equations for the complex field envelope A, saturable gain G, and saturable loss Q:

$$\gamma^{-1}\frac{dA}{dt} + A = \sqrt{\kappa}\big[e^{-Q/2}A\,(t-\tau) + P_{0g}\big], \tag{25}$$

$$\frac{dG}{dt} = g_0 - \gamma_g G - \left(|e^{-Q/2}A(t-\tau) + P_{0g}|^2 - e^{-Q}|A(t-\tau)|^2\right), \tag{26}$$

$$\frac{dQ}{dt} = q_0 - \gamma_q Q - s\left(1 - e^{-Q}\right)|A\,(t-\tau)|^2. \tag{27}$$

Combining these three equations with Eqs. (20) and (21) evaluated at $\omega_{0g} = 0$ we get DDE model of a laser with inhomogeneously broadened gain line and adiabatically eliminated polarization in the absorbing medium. The lasing threshold in this laser can be expressed as

$$\sqrt{\kappa}\exp\left(\frac{g_0}{2\gamma_g} - \frac{q_0}{2\gamma_q}\right) = 1 + \frac{\sigma_g^2}{\tilde{\Gamma}^2}\left[1 - \sqrt{\kappa}\exp\left(-\frac{q_0}{2\gamma_q}\right)\right] \geq 1,$$

where $\tilde{\Gamma}^2 = \Gamma_g \left[\Gamma_g + \sigma_g p_{2g}\right]$, i.e. inhomogeneous broadening in the gain medium leads to an increase of the lasing threshold.

Similarly to Eqs. (25)-(27) the equations governing the time evolution of the complex field envelope A and saturable gain G can be derived for the case when inhomogeneous broadening is present in the absorber medium only. Setting $\sigma_g = \omega_{0g} = \omega_{0q} = 0$, $P_{1g} = 0$, and eliminating adiabatically the variable P_{0g} we get $P_{0g} = \left(e^{G/2} - 1\right)\left[A(t-\tau) + P_{0q}\right]$ and

$$\gamma^{-1}\tfrac{dA}{dt} + A = \sqrt{\kappa}\left[e^{G/2} A\left(t-\tau\right) + P_{0q}\right], \tag{28}$$

$$\tfrac{dG}{dt} = g_0 - \gamma_g G - \left(e^{G} - 1\right)\left|A\left(t-\tau\right) + P_{0q}\right|^2. \tag{29}$$

Combining these two equations with Eqs. (18), (19) and (22) evaluated at $\omega_{0q} = 0$ to these two equations we get the DDE model of a laser with inhomogeneously broadened absorber and homogeneously broadened gain lines. The lasing threshold of the central mode in this case can be expressed as

$$\sqrt{\kappa}\exp\left(\frac{g_0}{2\gamma_g} - \frac{q_0}{2\gamma_q}\right) = \frac{1 + \sigma_q^2/\tilde{\Gamma}^2}{1 + \sigma_q^2 e^{q_0/(2\gamma_q)}/\tilde{\Gamma}^2} \leq 1,$$

where $\tilde{\Gamma}^2 = \Gamma_q \left[\Gamma_q + \sigma_q p_{2q}\right]$, i.e. inhomogeneous broadening in the absorber medium leads to a decrease of the linear threshold of the central mode located in the middle of the spectral profile of the absorption line.

4 Numerical results

4.1 TWE model

We solve equations (8)-(10) for the two-section laser with a gain and an absorber section using the discretization scheme similar to the one reported in [26, 27]. Since the number of moments reaches up to $M = 200$, we use parallelization techniques to speed up our simulations.

In numerical simulations the parameter values of Eqs. (8)-(10) were similar to those used earlier for modelling of monolithic semiconductor lasers with homogeneously broadened gain and absorption lines [26, 27]. In particular, the reflectivities of the laser facets were assumed to be equal, $\kappa_1 = \kappa_2 = 0.3$. Furthermore, for simplicity we assume that $\omega_{g0} = \omega_{q0} = 0$ and that all the linear losses take place on the laser facets, i.e., $\beta_{g,q} = 0$. The remaining parameters of the gain (absorber) sections are: normalized pump rate $n_0 = 10$ ns^{-1} (linear absorption rate $n_0 = 0.16$ ps^{-1}), longitudinal relaxation time $\gamma_N^{-1} = 1$ ns ($\gamma_N^{-1} = 10$ ps), transverse relaxation time $\Gamma^{-1} = 250$ fs ($\Gamma^{-1} = 250$ fs), and normalized saturation parameter $s = 1$ ($s = 5$). The length of the gain and absorber sections normalized to the group velocity of light in this sections are 10 ps and 2.5 ps, respectively.

A typical bifurcation tree obtained by plotting local maxima of the laser intensity time trace calculated for increasing values of the pump parameter n_0 in the gain medium in a laser with homogeneously broadened gain and absorber lines, $\sigma_g = \sigma_q = 0$, is shown by cyan circles in Figure 1. It can be seen that soon after the lasing threshold a regime with periodic laser intensity undergoes an instability leading to a Q-switched mode-locking regime corresponding to a cloud of points in Fig. 1. Quasiperiodic intensity time trace of the latter regime is shown in the top panel of Fig. 2. At even larger pumps a fundamental mode-locking regime illustrated in the bottom panel of Fig. 2 becomes stable. Black rectangles (blue triangles) in Fig. 1 are obtained by increasing the pump parameter n_0 at fixed and equal inhomogeneous broadening linewidths, $\sigma_g = \sigma_q = \sigma$, in the gain and absorber media, $\sigma = 2$

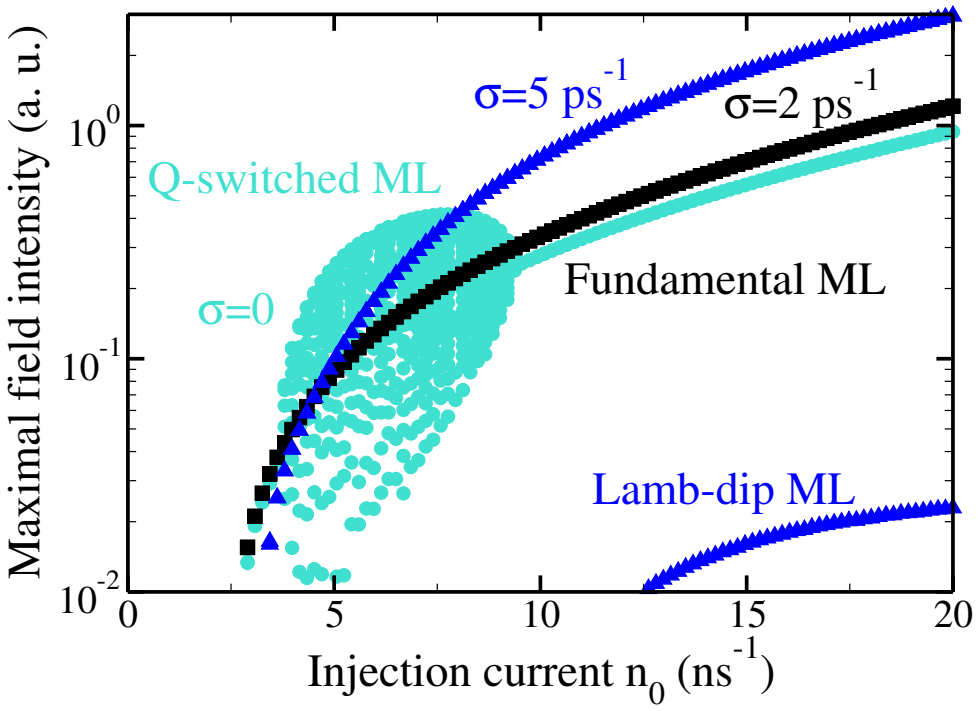

Figure 1: Bifurcation tree obtained by numerical integration of Eqs. (8)-(10). Local maxima of the field intensity are plotted for different values of the pump parameter n_0 in the gain medium. Cyan circles correspond to $\sigma = 0$, black rectangles – to $\sigma = 2$ ps^{-1}, and blue triangles – to $\sigma = 5$ ps^{-1} in a laser with inhomogeneously broadened gain and absorber lines. Blue triangles in the lower right corner of the figure indicate the peak power of the satellite pulse that appears at the trailing edge of the main pulse. Other parameter values are given in the beginning of Sec. 4.1.

ps^{-1} ($\sigma = 5$ ps^{-1}). It can be seen that the lasing threshold remains almost independent of σ, however, the Q-switching instability is gone for $\sigma \geq 2$ ps^{-1}. Therefore, we conclude that inhomogeneous broadening can lead to a suppression of this instability, which is in agreement with the experimental data on quantum-dot mode-locked lasers [28] and with the general considerations of Ref. [15].

For sufficiently large σ in the gain and absorber media small satellite pulses can appear at the trailing edge of the main mode-locked pulse. This can be seen in Fig. 3(a) illustrating fundamental mode-locking regimes with one, two and three additional satellite pulses. The corresponding spectra shown in Fig. 3(b) become wider with the increase of σ and eventually a Lamb dip, similar to that reported earlier in actively mode-locked quantum-dot laser [15], is formed in the middle of the pulse spectrum. Further increase of the inhomogeneous line width leads to a separation of the spectral comb into two symmetric combs with positive and negative central frequencies and subsequent degradation of mode-locking.

Evolution of fundamental mode-locked regime with the increase of the inhomogeneous broadening widths σ in the gain and absorber media is illustrated by Fig 4(a). Black circles in this figure indicate local maxima of the field intensity calculated for different values of σ with fixed normalized pump parameter $n_0 = 10$ ns^{-1}. It can be seen that the peak power of the mode-locked pulse increases with σ within the interval $\sigma \in [0, 5]$ ps^{-1}, while for $\sigma > 5$ ps^{-1} additional satellite pulses shown in Fig. 3(a) appear on the trailing edge of the pulse. Blue line in Fig. 4(a) indicates the linear increase of the pulse intensity with the homogeneous broadening width Γ in the absence of inhomogeneous broadening, $\sigma = 0$. Figure 4(b) presents a similar bifurcation diagram calculated for smaller value of the pump parameter, $n_0 = 6$ ns^{-1} corresponding to a stable Q-switched mode-locking regime in the absence

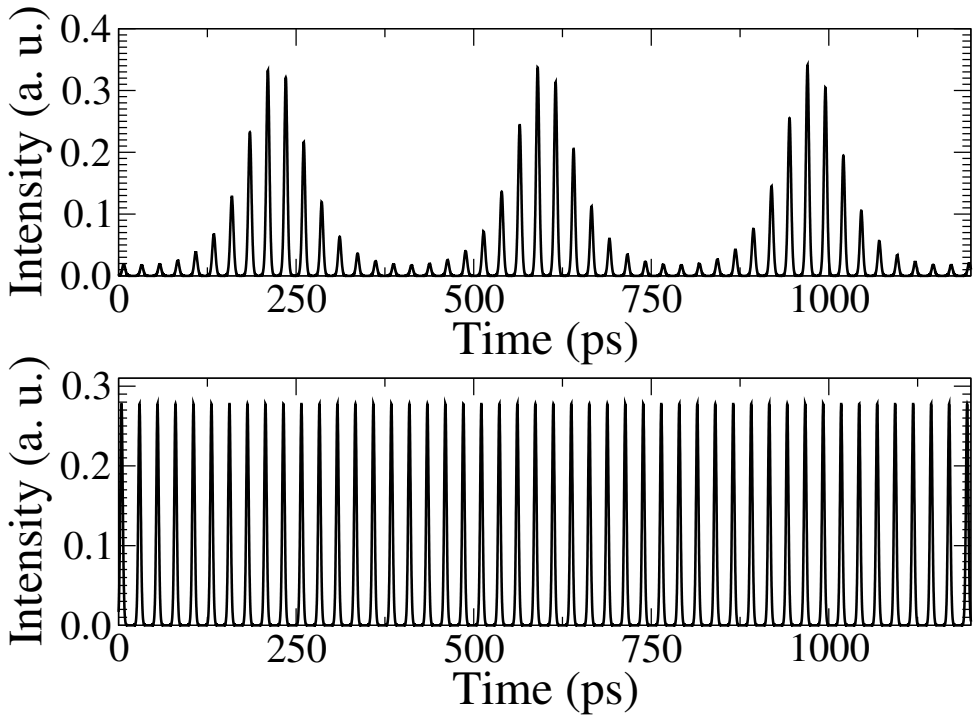

Figure 2: Right: Time traces of Q-switched regime (top) and fundamental mode-locking regime (bottom) calculated for $\sigma = 0$. Other parameter values are as in Fig. 1.

of inhomogeneous broadening. It can be seen that increasing the inhomogeneous broadening width in the gain medium up to $\sigma \approx 2$ ps^{-1} leads to a suppression of Q-switching instability and a transition to a stable fundamental mode-locking regime. The latter regime remains stable for $2 \leq \sigma < 6$ ps^{-1}.

It follows from Fig. 5 that the Lamb-dip instability appears due to the inhomogeneous broadening of the gain line, while the suppression of Q-switching is due to inhomogeneous broadening of the absorber line, see Fig. 5(b). The absence of instability for high values of the parameter σ in the absorber medium (see top panel of Fig. 5(b)) suggests that the inhomogeneous broadening in the absorber medium does not participate in the development of Lamb-dip instability. On the other hand, the diagram shown in bottom panel of Fig. 5(b) indicates that inhomogeneous broadening of the gain medium does not suppress the Q-switching instability of mode-locked regime, but on the contrary enhances this instability.

In order to study the effect of the inhomogeneous broadening in the gain and absorber media on the characteristics of mode-locked pulses we plot in Fig. 6 the dependence of their full-width at half-maxima, spectral width, energy, and the time-bandwidth product as functions of the inhomogeneous broadening width σ. It can be seen from this figure that the pulse width decreases and the spectral width increases with increasing σ. This is in agreement with intuitive expectations as well as with the theoretical results obtained for actively mode-locked quantum-dot lasers [15]. The time-bandwidth product remains almost constant for $\sigma < 5$ ps^{-1}, and increases drastically together with the spectral width for higher σ. The pulse energy decreases monotonically with increasing σ.

Finally, one can notice from Fig. 1 that an increase of inhomogeneous broadening linewidth σ can lead to a slight increase the lasing threshold. Fig. 6(a) shows a more dramatic increase of the lasing threshold obtained for faster gain relaxation rate $\gamma = 125$ ps^{-1}. Furthermore, a comparison of Fig. 6(b) and Fig. 1 shows that for the faster gain relaxation rate $\gamma = 125$ ps^{-1} the Lamb-dip instability of mode-locking regime appears at higher values of σ then for slower relaxation rate $\gamma = 10$ ps^{-1}.

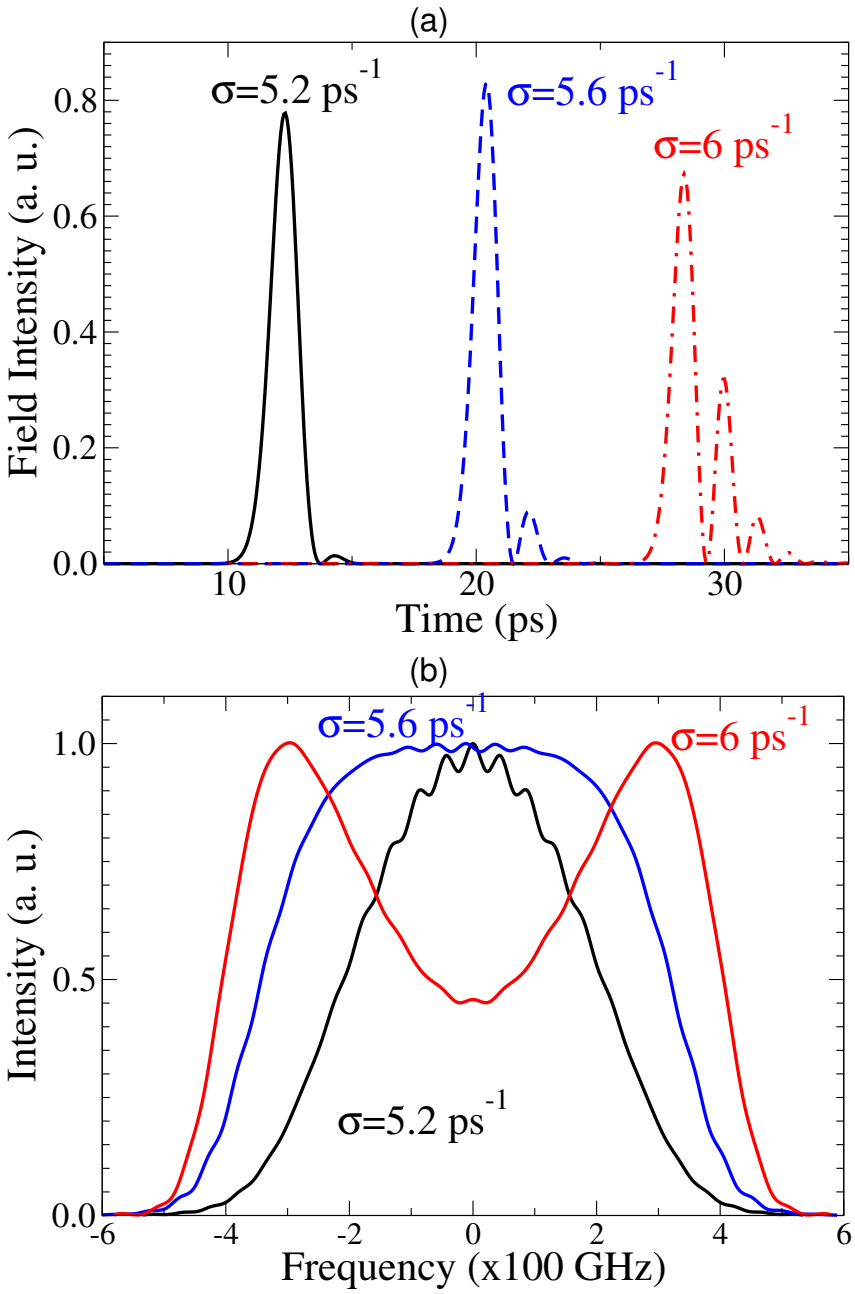

Figure 3: Pulses (a) and optical spectra (b) in a laser with inhomogeneously broadened gain and absorber lines having equal linewidth $\sigma = 5.2$ ps, $\sigma = 5.6$ ps, and $\sigma = 6$ ps. Other parameters are as in Fig. 1.

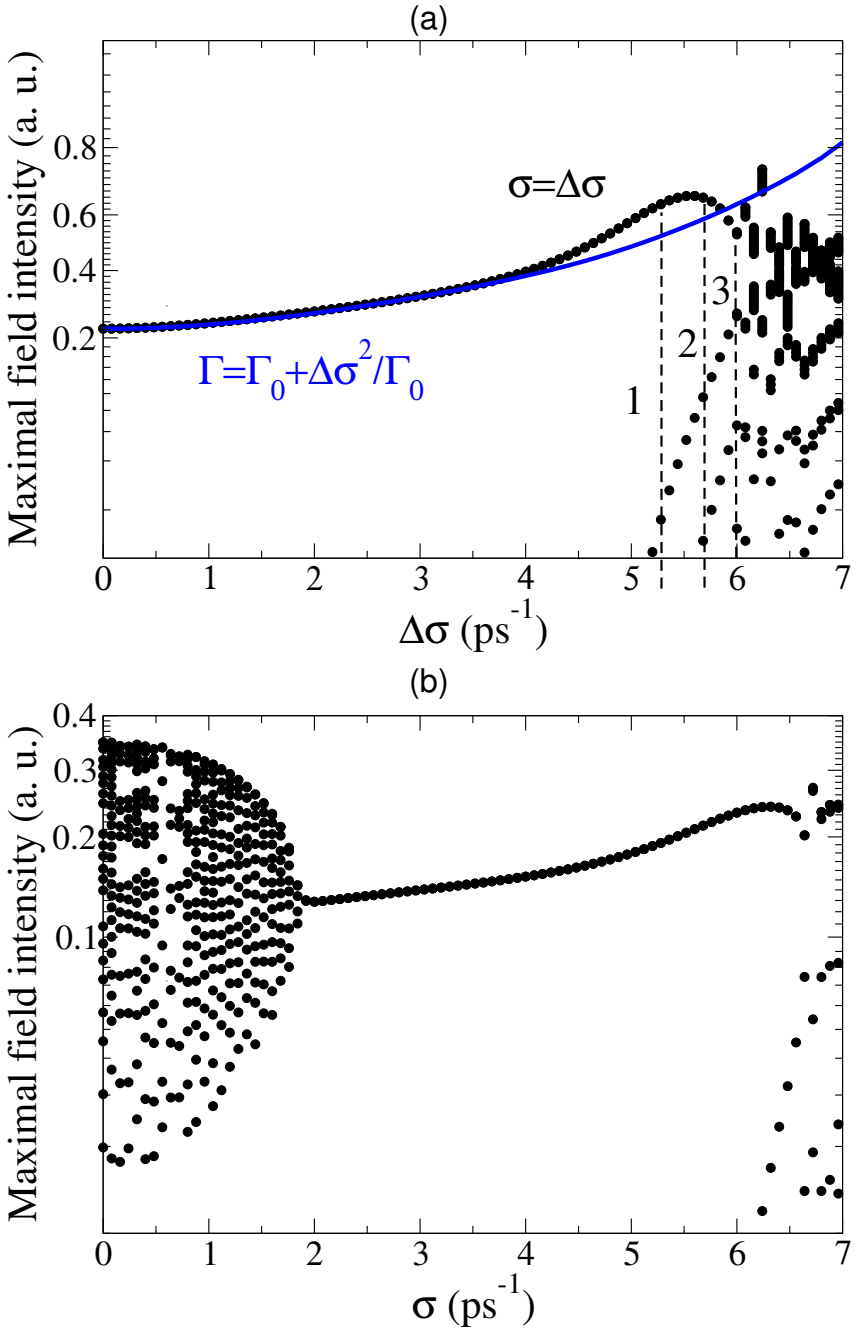

Figure 4: Bifurcation diagrams similar to that shown in Fig. 1, obtained by increasing the parameter σ in both media. (a): Black dots show local maxima of the field intensity calculated by changing σ with fixed normalized pump rate $n_0 = 10$ ns^{-1}. Blue line represents intensity maxima of fundamental mode-locking solutions calculated by changing $\Gamma_g = \Gamma_q$ in a laser with homogeneously broadened gain and absorption lines. Dashed lines denote values of σ where new satellite pulses appear. (b): Same as black dots in the upper panel, but for $n_0 = 6$ ns^{-1}. Other parameters are as in Fig. 1.

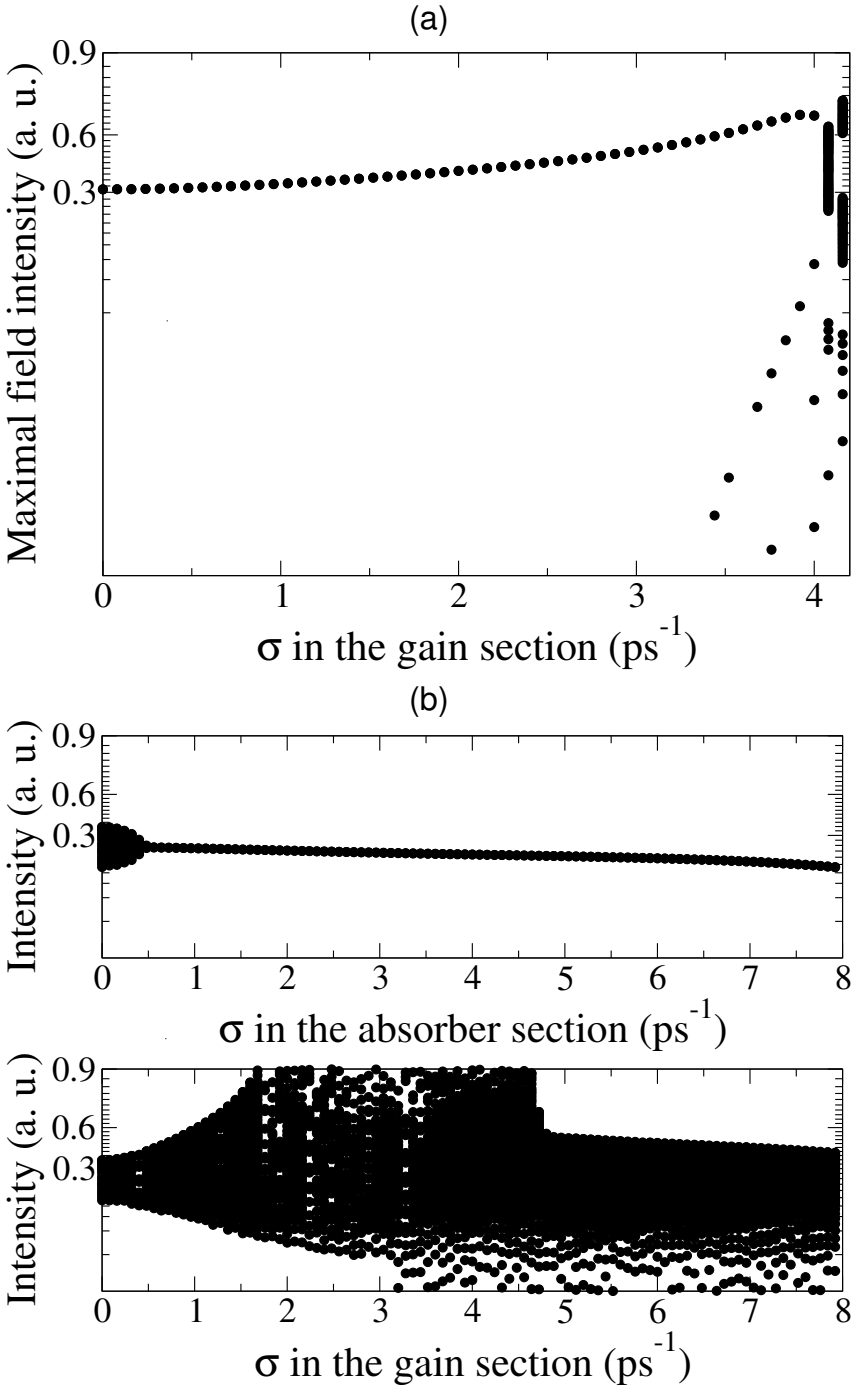

Figure 5: Top: Bifurcation diagram obtained numerically by changing the parameter σ in the gain medium in a laser with homogeneously broadened absorption line. Normalized pump rate $n_0 = 20$ ns^{-1}. Bottom: Bifurcation diagram obtained numerically by changing the parameter σ in the absorber medium in a laser with homogeneously broadened gain line (top) and the parameter σ in the gain medium in a laser with homogeneously broadened absorption line. Normalized pump rate $n_0 = 9$ ns^{-1}. Other parameters are as in Fig. 1.

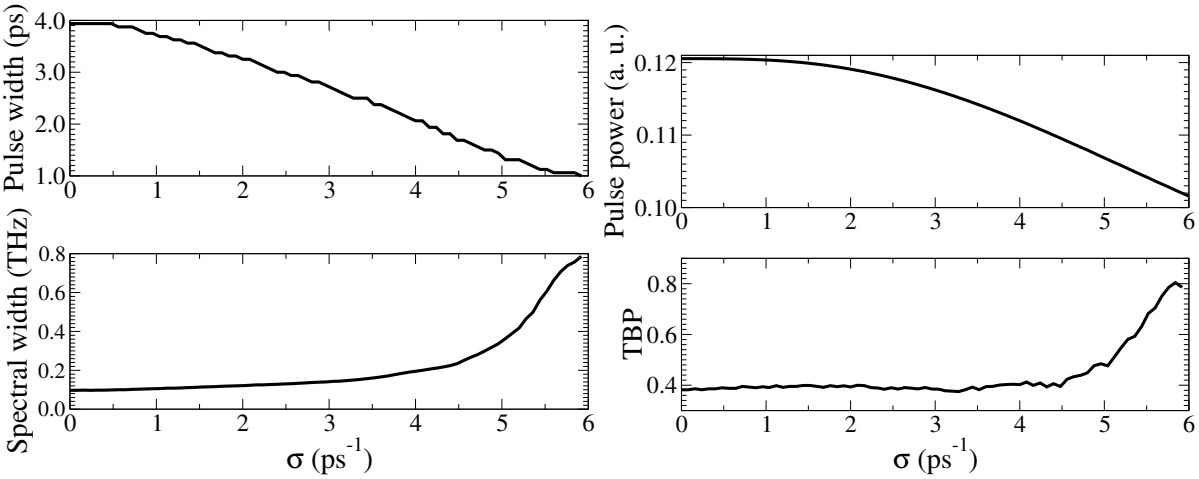

Figure 6: Left: Full-width at half-maximum of the mode-locked pulses (top) and their spectral width (bottom) as functions of equal inhomogeneous broadening widths σ in the gain and absorber media. $n_0 = 10$ ns^{-1} in the gain medium. Other parameters are as in Fig. 1. Right: Pulse energy (top) and time-bandwidth product versus inhomogeneous broadening linewidth in the gain medium. $n_0 = 10$ ns^{-1} in the gain medium. Other parameters are as in Fig. 1.

4.2 DDE model

First, we simulate the DDE model (12)-(16) of a laser with inhomogeneously broadened gain and absorption lines with the parameter values close to those of the TWE model: $\tau = 25$ ps, $\kappa = 0.3$, $\gamma_g^{-1} = 1$ ns, $\gamma_q^{-1} = 5$ ps, $\Gamma_g^{-1} = \Gamma_q^{-1} = 250$ fs, $\gamma^{-1} = 25$ fs, $s = 10$, $g_0 = 6$ ns^{-1}, and $q_0 = 0.1$ ps^{-1}. The dependence of the pulse peak intensity on the inhomogeneous broadening width $\sigma_g = \sigma_q \equiv \sigma$ obtained with the help of the DDE-BIFTOOL software package [29] is presented in Fig. 8(a). It can be seen that the bifurcation diagram in this figure is similar to that obtained by numerical simulation of the TWE model, see Fig. 4(b).

In order to perform numerical analysis of the Lamb-dip instability we simulate the DDE model with inhomogeneously broadened gain line and adiabatically eliminated polarization in the absorber medium, Eqs. (25)-(27), (20), and (21). We increase carrier relaxation rate up to $\gamma_g^{-1} = 500$ ps and, using the DDE-BIFTOOL software package, perform a continuation of the mode-locked solution along the parameter σ_g, see Fig. 8(b). The presence of additional lines in the bottom right corner of the figure indicates that similarly to the results of numerical simulation with the TWE model shown in Fig. 4(b) the increase of σ_g leads to formation of small satellite pulses behind the main mode-locked pulse. The branch of mode-locked solutions in Fig. 4(b) ends up at a saddle-node (fold) bifurcation point, where the negative real eigenvalue with smallest absolute value becomes zero. At this point the stable fundamental mode-locking solution annihilates with an unstable one.

Figure 9(a) presents a branch of mode-locking solutions of the DDE model (28), (29), (18),(19), and (22) homogeneously broadened absorber line and adiabatically eliminated polarization in the gain medium. The part of this branch between bifurcation points A and B shown by dotted line is unstable with respect to Q-switching instability. In Fig. 9(b) the critical values of the pump parameter g_0 corresponding to the Q-switching instability bifurcation points are shown as functions of the inhomogeneous broadening width $\sigma_q = \sigma$ of the absorption line. It can be seen that with increasing σ the two bifurcation points collide and disappear, and the mode-locking solution branch becomes stable within the whole range of pump parameters shown in Fig. 9(a).

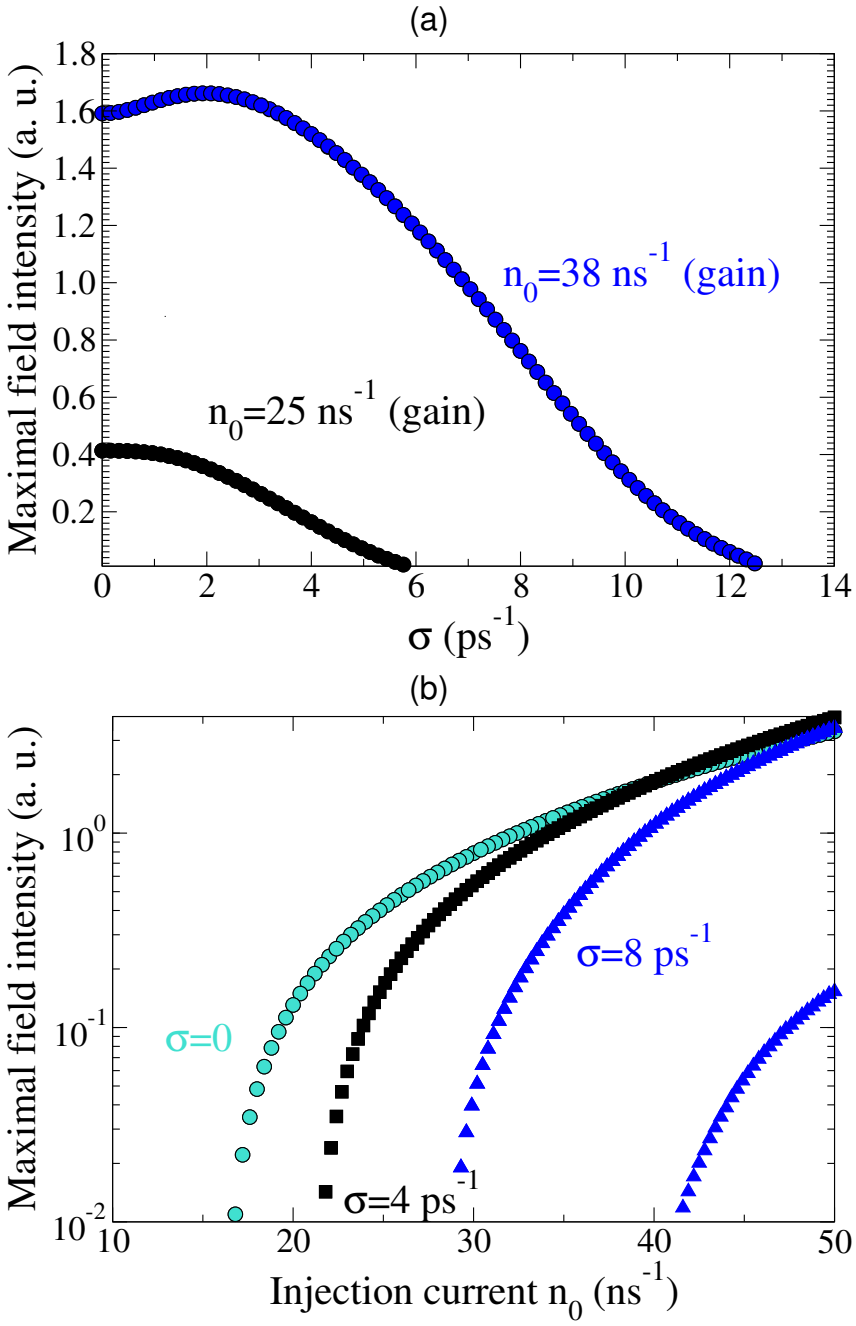

Figure 7: (a) Bifurcation diagram obtained numerically by changing the parameter σ in both media for pump rates $n_0 = 25$ ns^{-1} and 38 ns^{-1} in the gain medium. (b) Bifurcation diagram obtained numerically by changing the parameter n_0 in the gain medium for $\sigma = 0$ (circles), $\sigma = 4$ ps^{-1} (rectangles), and $\sigma = 8$ ps^{-1} (triangles) in both media, $\gamma_N = 125$ ps^{-1} in the gain medium, $n_0 = -320$ ns^{-1} in the absorber medium. Other parameters are as in Fig. 1.

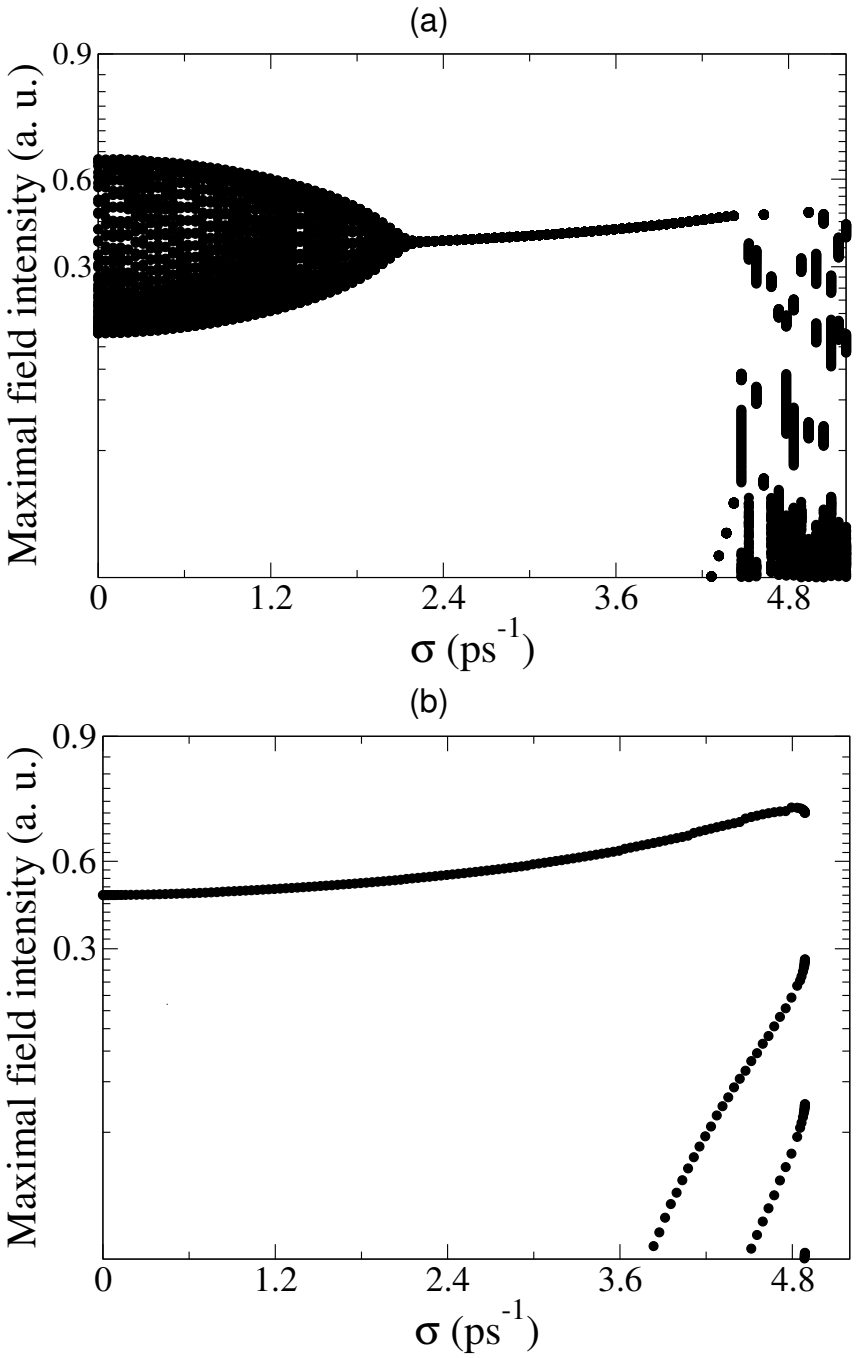

Figure 8: (a) Bifurcation diagram obtained numerically by changing the parameter $\sigma_g = \sigma_q = \sigma$ in both laser media using the DDE model (12)-(16). (b) Bifurcation diagram obtained with the help of DDE-BIFTOOL by changing the parameter $\sigma_g = \sigma$ in the DDE model (25)-(27), (20), and (21). Other parameters can be found in the beginning of Section 4.2.

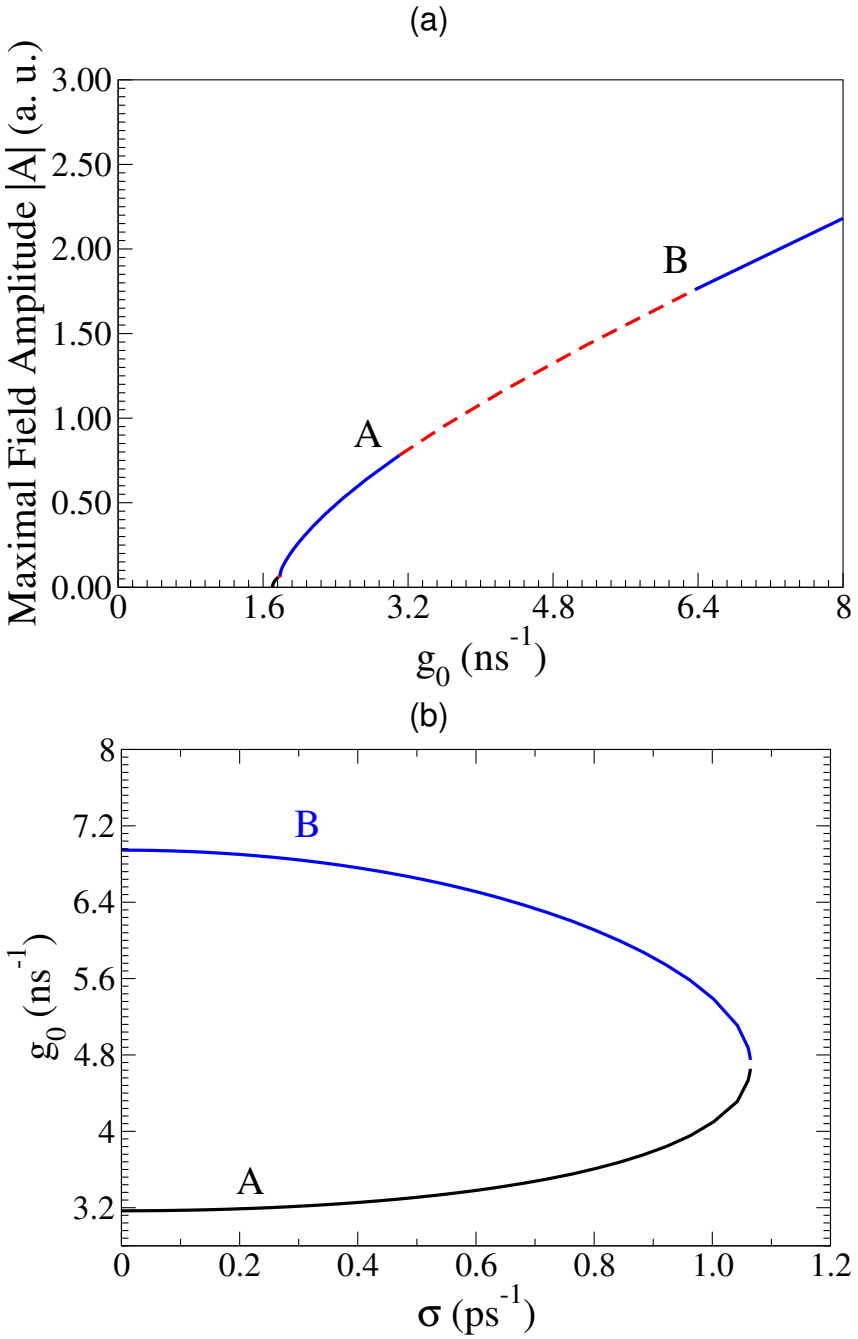

Figure 9: (a) Bifurcation diagram obtained using the DDE-BIFTOOL by continuing the branch of the mode-locking regime along the parameter g_0 of the DDE model (28), (29), (18), (19), and (22) with $\sigma_q = 0$. Solid lines indicate stable solutions, while dashed line indicates unstable ones. $\gamma^{-1} = 250$ ns. (b) Two-parameter bifurcation diagram obtained using the DDE-BIFTOOL by following the Q-switching instability bifurcation points A and B along the parameter $\sigma_q = \sigma$ of the DDE model (28), (29), (18), (19), and (22). Other parameter are as in Fig. 8.

5 Conclusion

We have studied numerically two-level TWE model of a passively mode-locked laser with inhomogeneousy broadened gain and absorption lines. We have proposed an efficient spectral method for numerical integration of this model, and implemented this method using parallel computation techniques. We have studied the effect of the inhomogeneous broadening on the characteristics of the fundamental mode-locking regime. It follows from our analysis that, alongside with the carrier dynamics processes in the gain medium, see e.g. [27, 28, 30], inhomogeneous broadening may lead to a suppression of Q-switching instability in mode-locked quantum-dot lasers. This is in agreement with qualitative considerations, which suggest the enhancement of the gain saturation and suppression of Q-switching due to inhomogeneous broadening [31]. We have shown that equal inhomogeneous broadening widths in both laser media can lead to the increase of the lasing threshold, pulse intensity and spectral width, and to the decrease of the pulse width and the pulse power. Moreover, small inhomogeneous broadening has the effect on pulse characteristics similar to that of homogeneous broadening, whereas large inhomogeneous broadening in the absorber (gain) medium leads to a suppression of Q-switching instability (the formation of the Lamb dip in the spectral profile of the pulse and the degradation) of the mode-locking regime. We have demonstrated that the increase of the longitudinal relaxation rate in the gain medium leads to stabilization of the fundamental mode-locking regime for strong inhomogeneous broadening and to further increase of the lasing threshold.

We have derived a simplified DDE model of an inhomogeneously broadened laser which demonstrates dynamical behavior qualitatively similar to that of the TWE model. Using the DDE model we have shown that the degradation of mode-locked regime at sufficiently large values of the inhomogeneous broadening linewidth in the gain medium takes place after a fold bifurcation where the stable branch of fundamental mode-locked solutions collides with unstable one and disappears. Finally, we have demonstrated that with the increase of inhomogeneous broadening linewidth in the absorber medium two bifurcation points responsible for the appearance to the Q-switching instability of mode-locked regime collide and disappear, leading to elimination of this instability by inhomogeneous broadening.

Appendix A. DDE model

To derive a DDE model of a ring passively mode-locked laser taking into account medium polarization dynamics we use the approach similar to that proposed in [22–24]. We start with the unidirectional travelling wave equations describing the space-time evolution of the complex electrical field envelope E, complex two-level polarization P, and real population difference N in the gain and absorber media written out in co-moving coordinate frame $z + t \to z$, $t \to t$:

$$\frac{\partial E}{\partial z} = P,$$
$$\frac{\partial P}{\partial t} = (-\Gamma + i\omega)P + \frac{\Gamma}{2}EN,$$
$$\frac{\partial N}{\partial t} = n_0 - \gamma_N n - s(EP^* + PE^*) = n_0 - \gamma_N n - s\frac{\partial |E|^2}{\partial z},$$

where the equation for the electric field envelope E can we rewritten in the form:

$$\frac{\partial^2 E}{\partial t \partial z} + (\Gamma - i\omega)\frac{\partial E}{\partial z} = \frac{\Gamma}{2}EN. \tag{30}$$

Assuming that the time evolution of the population difference N is much slower than that of the field envelope E we apply Fourier-transform to (30) considering $N(t,z)$ to be independent of time t. Then we obtain

$$2\pi i\xi\frac{d\tilde{E}}{dz}+(\Gamma-i\omega)\frac{d\tilde{E}}{dz}=\frac{\Gamma}{2}\tilde{E}N. \tag{31}$$

Integrating (31) along longitudinal coordinate z from the point z_1 at the beginning of the gain/absorber medium to the point z_2 at the end of the the medium we get

$$\tilde{E}(\xi,z_2)=\exp\left[\frac{\Gamma G}{2(\Gamma-i\omega+2\pi i\xi)}\right]\tilde{E}(\xi,z_1)= \\ \sum_{k=0}^{\infty}\frac{1}{k!}\left[\frac{\Gamma G}{2(\Gamma-i\omega+2\pi i\xi)}\right]^k\tilde{E}(\xi,z_1), \tag{32}$$

where $\tilde{G}(t,z)=\int_{z_1}^{z}Ndz$, $G(t)=G(t,z_2)$. Therefore, by making the inverse Fourier transform of (32) we obtain

$$E(t,z_2)=E(t,z_1)+ \\ \frac{\Gamma G(t)}{2}\int_{-\infty}^{t}E(s,z_1)e^{(\Gamma-i\omega)(s-t)}\frac{I_1\left[\sqrt{G(t)(t-s)\frac{2\Gamma}{\Gamma-i\omega}}\right]}{\sqrt{G(t)(t-s)\frac{\Gamma}{2(\Gamma-i\omega)}}}ds, \tag{33}$$

where I_1 is the first order Bessel function. Here, we note that since $\frac{1}{\Gamma}\frac{\partial E}{\partial t}\sim 1$ for large $\Gamma\gg 1$, the error introduced by our approximation by non-constant but relatively slow $N(t)$ with $\frac{\partial N}{\partial t}\sim 1$ can be roughly estimated as $\frac{1}{\Gamma}\frac{\partial^2 E}{\partial t\partial z}+(1-i\frac{\omega}{\Gamma})\frac{\partial E}{\partial z}-\frac{NE}{2}=\frac{1}{\Gamma N}\left(\frac{\partial N}{\partial t}\frac{\partial E}{\partial z}+\frac{\partial\tilde{G}}{\partial t}(\frac{\partial^2 E}{\partial z}-\frac{1}{N}\frac{\partial N}{\partial z}\frac{\partial E}{\partial z})\right)\ll 1$, which is small for $\Gamma\gg 1$.

Finally, assuming that the time evolution of $G(t)$ is slow we eliminate distributed delay we rewrite Eq. (33) as the following chain of equations

$$E(t,z_2)=E(t,z_1)+P_1(t),$$
$$\frac{dP_1(t)}{dt}=(-\Gamma+i\omega)P_1(t)+\frac{\Gamma G(t)}{2}(E(t,z_1)+P_2(t)),$$
$$\frac{dP_2(t)}{dt}=(-\Gamma+i\omega)P_2(t)+\frac{\Gamma G(t)}{2\times 2}(E(t,z_1)+P_3(t)),$$
$$\frac{dP_3(t)}{dt}=(-\Gamma+i\omega)P_3(t)+\frac{\Gamma G(t)}{3\times 2}(E(t,z_1)+P_4(t)),$$
$$\dots$$
$$\frac{dP_k(t)}{dt}=(-\Gamma+i\omega)P_k(t)+\frac{\Gamma G(t)}{2k}(E(t,z_1)+P_{k+1}(t)),$$
$$\dots$$

where P_m are auxiliary variables describing the polarization at the point z_2. Assuming $G(t)/2\ll 1$, we can truncate the system at any $k\geq 1$. For higher $G(t)\sim 1$ we improve the approximation by keeping a single polarization equation for P_1 with all other auxiliary variables P_m ($m>1$) eliminated adiabatically:

$$\frac{dP_1(t)}{dt}=(-\Gamma+i\omega)P_1(t)+\Gamma(e^{G(t)/2}-1)E(t,z_1).$$

This equation is responsible for nonlinear spectral filtering approximating the effect of two-level polarization on the laser dynamics at small $G(t)$.

Using the above approximation, we write the following equation for the time evolution of the complex electric field envelope in a two-section passively mode-locked laser

$$\frac{dA}{dt} + (\gamma - i\omega_0)A = \sqrt{\kappa}\gamma\left[A\left(t-\tau\right) + P_q(t) + P_g(t)\right], \tag{34}$$

where $P_g(t)$ and $P_q(t)$ describe the polarization of the gain and absorber medium, respectively. Equation (34) together with Eqs. (13)-(16) gives us a DDE model for a homogeneously broadened mode-locked laser . By setting $\omega_{0g} = \omega_{0q} = 0$ and performing adiabatic elimination of the variables P_g and P_q we obtain from this model the standard DDE mode-locking model of Refs. [22–24].

Appendix B. Energy estimates

Performing the coordinate change (7), projecting Eqs. (2) and (3) with the help of inner product (6) onto $P^{\pm}\psi_0$ and $N\psi_0$, respectively, and summing the resulting three equations, we obtain the following equation for the sum of the L^2 norms $\|\cdot\| = \langle\cdot,\cdot\rangle$

$$\begin{aligned}\frac{1}{2}\frac{\partial(\|\hat{N}\|^2 + \|\hat{P}^+\|^2 + \|\hat{P}^-\|^2)}{\partial t} = \left\langle n_0, \hat{N}\right\rangle - \\ \gamma_N\|\hat{N}\|^2 - \Gamma(\|\hat{P}^+\|^2 + \|\hat{P}^-\|^2),\end{aligned} \tag{35}$$

where the nonlinear terms cancelled each other out after summation. Without loss of generality, we can make physically relevant assumption $\gamma_N < \Gamma$ to obtain the following estimate for the quantity $\Psi = \left(\|\hat{N}\|^2 + \|\hat{P}^+\|^2 + \|\hat{P}^-\|^2\right)^{1/2}$

$$\Psi(t,z) \le \Psi_0(z)\exp(-\gamma_N t) + \frac{1-\exp(-\gamma_N t)}{\gamma_N}\|n_0(\omega,z)\| \tag{36}$$

for all $z \in [0,l]$, where $\Psi_0(z) = \left(\|\hat{N}(\omega,0,z)\|^2 + \|\hat{P}^+(\omega,0,z)\|^2 + \|\hat{P}^-(\omega,0,z)\|^2\right)^{1/2}$.

Similarly to Eq. (35) for each $m = 0, 1, \ldots, M$ we can obtain the following equation for time evolution of the sum of L^2 norms $\Psi_m = (|N_m|^2 + |P_m^+|^2 + |P_m^-|^2)^{1/2}$ of the solutions of Eqs. (8)-(10) :

$$\begin{aligned}\frac{1}{2}\frac{\partial\Psi_m^2}{\partial t} = n_{0m}N_m - \Gamma\left(|P_m^+|^2 + |P_m^-|^2\right) - \gamma_N N_m^2 + \\ \mathrm{Re}\big[i\sigma\big(\sqrt{m}(P_{m-1}^+P_m^{+*} + P_{m-1}^-P_m^{-*}) + \\ \sqrt{m+1}(P_{m+1}^+P_m^{+*} + P_{m+1}^-P_m^{-*})\big)\big],\end{aligned} \tag{37}$$

where $P_{-1}^{\pm} \equiv P_{M+1}^{\pm} \equiv \Psi_{-1} \equiv \Psi_{M+1} \equiv 0$.

Next, using the right-hand side of Eq. (37) we obtain an estimate from above for Ψ_m^2. First, for every m for the sake of convenience we introduce an auxiliary function

$$p(m,k) = \begin{cases} 1, & m \le 0, \\ m^k, & m > 0 \end{cases}$$

Then rescaling the variables $\hat{P}_m^{\pm} = p(m,k)P_m^{\pm}$, $N_m = p(m,k)N_m$, and $\hat{\Psi}_m = p(m,k)\Psi_m$ and multiplying Eq. (37) by $p(m,2k)$ we obtain

$$\begin{aligned}\frac{1}{2}\frac{\partial\hat{\Psi}_m^2}{\partial t} = p(m,k)n_{0m}\hat{N}_m - \Gamma(|\hat{P}_m^+|^2 + |\hat{P}_m^-|^2) - \gamma_N\hat{N}_m^2 + \\ \mathrm{Re}\Bigg[i\sigma\Bigg(\sqrt{m}\frac{p(m,k)}{p(m-1,k)}(\hat{P}_{m-1}^+\hat{P}_m^{+*} + \hat{P}_{m-1}^-P_m^{-*}) + \\ \sqrt{m+1}\frac{p(m,k)}{p(m+1,k)}(\hat{P}_{m+1}^+\hat{P}_m^{+*} + \hat{P}_{m+1}^-\hat{P}_m^{-*})\Bigg)\Bigg].\end{aligned} \tag{38}$$

Next, summing equations (38) over all m in the range $M_0 \le m \le M$ we derive an equation for the time evolution of the sum $\hat{\Psi}_\Sigma^2 = \sum_{m=M_0}^{M}\hat{\Psi}_m^2$:

$$\begin{aligned}\frac{1}{2}\frac{\partial\hat{\Psi}_\Sigma^2}{\partial t} = \frac{1}{2}\frac{\partial\sum_{m=M_0}^{M}\hat{\Psi}_m^2}{\partial t} = \sum_{m=M_0}^{M} p(m,k)n_{0m}\hat{N}_m + \\ \mathrm{Re}\left[i\sigma\sqrt{M_0}\frac{p(M_0,k)}{p(M_0-1,k)}\left(\hat{P}_{M_0-1}^+\hat{P}_{M_0}^{+*} + \hat{P}_{M_0-1}^-\hat{P}_{M_0}^{-*}\right)\right] + \\ \sum_{m=M_0+1}^{M}(R_m^+ + R_m^-) - \sum_{m=M_0}^{M}\left(\Gamma(|\hat{P}_m^+|^2 + |\hat{P}_m^-|^2) + \gamma_N\hat{N}_m^2\right),\end{aligned} \tag{39}$$

where, M_0 ($0 \le M_0 < M$) will be defined below and

$$\begin{aligned}R_m^{\pm} = \mathrm{Re}\, i\sigma\left[\sqrt{m}\frac{p(m,k)}{p(m-1,k)}\hat{P}_{m-1}^{\pm}\hat{P}_m^{\pm*} + \sqrt{m}\frac{p(m-1,k)}{p(m,k)}\hat{P}_m^{\pm}\hat{P}_{m-1}^{\pm*}\right] = \\ \frac{i\sigma\sqrt{m}}{2}\left[\frac{p(m,k)}{p(m-1,k)}\hat{P}_{m-1}^{\pm}\hat{P}_m^{\pm*} + \frac{p(m-1,k)}{p(m,k)}\hat{P}_m^{\pm}\hat{P}_{m-1}^{\pm*} - \right. \\ \left.\frac{p(m,k)}{p(m-1,k)}\hat{P}_{m-1}^{\pm*}\hat{P}_m^{\pm} - \frac{p(m-1,k)}{p(m,k)}\hat{P}_m^{\pm*}\hat{P}_{m-1}^{\pm}\right] = \\ c_{m,k}\,\mathrm{Re}\, i\sigma\hat{P}_{m-1}^{\pm}\hat{P}_m^{\pm*}\end{aligned}$$

with

$$c_{m,k} = \sqrt{m}\left[\frac{p(m,k)}{p(m-1,k)} - \frac{p(m-1,k)}{p(m,k)}\right]. \tag{40}$$

It follows from (40) that $c_{m,k} = 0$ when $k = 0$ or $m \le 1$. For $k, m > 0$ the quantity $c_{m,k}$ vanishes in the limit $m \to \infty$:

$$\begin{aligned}\lim_{m\to\infty} c_{m,k} = \lim_{m\to\infty}\sqrt{m}\left[\frac{m^k}{(m-1)^k} - \frac{(m-1)^k}{m^k}\right] = \\ \lim_{m\to\infty}\sqrt{m+1}\left[\frac{(m+1)^k}{m^k} - \frac{m^k}{(m+1)^k}\right] = \\ \lim_{m\to\infty}\sqrt{m+1}\frac{\left[\sum_{j=1}^{k}\frac{k!}{j!(k-j)!}m^{k-j}\right]\left[(m+1)^k + m^k\right]}{m^k(m+1)^k} = \\ \lim_{m\to\infty}\frac{\sqrt{m+1}}{m}\left[\sum_{j=1}^{k}\frac{k!}{j!(k-j)!}m^{1-j}\right]\left[1 + \left(\frac{m}{m+1}\right)^k\right] = 0.\end{aligned}$$

Therefore, we can find $M_0 > 0$ such that $|2\sigma c_{m,k}| < \Gamma/2$ for all $m > M_0$. Hence, for the quantities $R_m^{\pm}$ defined by (5) we get the following estimate:

$$R_m^{\pm} \le |R_m^{\pm}| \le |\sigma c_{m,k}| \left(|P_{m-1}^{\pm}|^2 + |P_m^{\pm}|^2\right) \le \frac{\Gamma}{2} \frac{|P_{m-1}^{\pm}|^2 + |P_m^{\pm}|^2}{2},$$

and, under non-restrictive assumption $\gamma_N < \Gamma/2$, the sum of two last terms in (39) satisfies the relations

$$\sum_{m=M_0+1}^{M} (R_m^+ + R_m^-) - \sum_{m=M_0}^{M} \Gamma \left(|\hat{P}_m^+|^2 + |\hat{P}_m^-|^2\right) + \gamma_N \hat{N}_m^2 \le$$
$$- \sum_{m=M_0}^{M} \frac{\Gamma}{2} \left(|\hat{P}_m^+|^2 + |\hat{P}_m^-|^2\right) + \gamma_N \hat{N}_m^2 \le -\gamma_N \hat{\Psi}_\Sigma^2.$$

Thus, we obtain from (39) the following inequality

$$\frac{1}{2} \frac{\partial \hat{\Psi}_\Sigma^2}{\partial t} \le \sigma \sqrt{M_0} \frac{p(M_0,k)}{p(M_0-1,k)} (|\hat{P}_{M_0-1}^+| + |\hat{P}_{M_0-1}^-|) \hat{\Psi}_\Sigma + \sum_{m=0}^{M} p(m,k) |n_{0m}| \hat{\Psi}_\Sigma - \gamma_N \hat{\Psi}_\Sigma^2. \tag{41}$$

Deviding both sides of (41) by $\hat{\Psi}_\Sigma$ and estimating the first term in the right-hand side using (36)

$$|\hat{P}_{M_0-1}^{\pm}| = p(M_0-1,k)|P_{M_0-1}^{\pm}| \le p(M_0-1,k)\|P^{\pm}\|\|\phi_{M_0-1}\| \le$$
$$p(M_0-1,k) \left(\|\Psi_0\| + \frac{1-\exp(-\gamma_N T)}{\gamma_N} \|n_0\|\right)$$

for all $t \in [0,T]$ we obtain the final differential inequality

$$\frac{\partial \hat{\Psi}_\Sigma}{\partial t} \le c_0 - \gamma_N \hat{\Psi}_\Sigma,$$

where c_0 satisfies (43). Therefore, according to a variant of a Gronwall's Lemma

$$\hat{\Psi}_\Sigma \le \left(\sum_{m=M_0}^{M} p(m,k) |\Psi_{0m}|^2\right)^{\frac{1}{2}} + c_0 \frac{1-e^{-\gamma_N T}}{\gamma_N}$$

for all $t \in [0,T]$. Finally, by using the relation $p(m,k)\Psi_m = \hat{\Psi}_m \le \hat{\Psi}_\Sigma$ we obtain

$$\Psi_m(t,z) \le m^{-k} \left[\left(\sum_{m=M_0}^{M} m^k |\Psi_{0m}(z)|^2\right)^{\frac{1}{2}} + c_0(z) \frac{1-e^{-\gamma_N T}}{\gamma_N}\right], \tag{42}$$

$$c_0 = \sigma M_0^{k+1/2} \left(\|\Psi_0\| + \frac{1-\exp(-\gamma_N T)}{\gamma_N} \|n_0\|\right) + |n_{00}| + \sum_{m=1}^{M} m^k |n_{0m}| \tag{43}$$

for all $t \in [0,T]$, $z \in [0,l]$, $M_0 \le m \le M$ with some $T > 0$, $M_0 > 0$, and integer $k > 0$ that can be chosen independently on M. For $n_{0m} = j_0 \delta_{0m}$ the sum in (43) is 0, and the initial values can be chosen so that the sum in (42) is bounded and converges with $M \to \infty$, hence this estimate implies that the moments vanish with $m \to \infty$.

References

[1] H. Schmeckebier, G. Fiol, C. Meuer, D. Arsenijević, and D. Bimberg, "Complete pulse characterization of quantum dot mode-locked lasers suitable for optical communication up to 160 gbit/s," *Opt. Express*, vol. 18, pp. 3415–3425, Feb 2010.

[2] D. Bimberg, M. Grundmann, and N. N. Ledentsov, *Quantum Dot Heterostructures*. Wiley, 1998.

[3] E. U. Rafailov, M. A. Cataluna, and W. Sibbett, "Mode-locked quantum-dot lasers," *Nature Photonics*, vol. 1, pp. 395–401, 2007.

[4] M. Grundmann, "The present status of semiconductor lasers," *Physica E*, vol. 5, p. 167, 2000.

[5] V. S. Idiatulin and A. V. Uspenskii, "The possibility of the existence of a pulsating mechanism related to inhomogeneous broadening in the lasing transition line," *Radio Eng. Electron. Phys.*, vol. 18, pp. 422–425, 1973.

[6] L. W. Casperson, "Stability criteria for high-intensity lasers," *Phys. Rev. A*, vol. 21, no. 3, pp. 911–923, 1980.

[7] R. Graham and Y. Cho, "Self-pulsing and chaos in inhomogeneously broadened single mode lasers," *Opt. Commun.*, vol. 47, no. 1, pp. 52 – 56, 1983.

[8] L.A.Lugiato, L.M.Narducci, D.K.Bandy, and N.B.Abraham, "Instabilities in inhomogeneously broadened single-mode lasers," *Opt. Commun.*, vol. 46, no. 2, pp. 115–120, 1983.

[9] P. Mandel, "Influence of Doppler broadening on the stability of monomode ring lasers," *Opt. Commun.*, vol. 44, no. 6, pp. 400–404, 1983.

[10] B. Meziane, "A simple model of the "Casperson instability" for a single mode inhomogeneously broadened laser," *Opt. Commun.*, vol. 75, no. 3-4, pp. 287 – 293, 1990.

[11] B. Meziane, "Inhomogeneously broadened laser modeling: strategies and validity of low-dimensional formulations of the maxwell-bloch equations," *Optics Communications*, vol. 128, pp. 377 – 384, 1996.

[12] E. Roldán, G. J. de Valcárcel, and F. Silva, "Multimode emission in inhomogeneously broadened ring lasers," *J. Opt. Soc. Am. B*, vol. 18, no. 11, pp. 1601–1611, 2001.

[13] E. Roldán and G. J. de Valcárcel, "Multimode instability in inhomogeneously broadened class-b ring lasers: Beyond the uniform-field limit," *Phys. Rev. A*, vol. 64, no. 5, p. 053805, 2001.

[14] F. Prati, E. M. Pessina, G. J. de Valcárcel, and E. Roldán, "Coherent effects in the multimode dynamics of inhomogeneously broadened ring lasers," *Opt. Commun.*, vol. 237, pp. 189–199, 2003.

[15] C. Xing and E. A. Avrutin, "Multimode spectra and active mode locking potential of quantum dot lasers," *J. Appl. Phys.*, vol. 97, no. 10, p. 104301, 2005.

[16] M. Rossetti, P. Bardella, and I. Montrosset, "Time-domain travelling-wave model for quantum dot passively mode-locked lasers," *IEEE J. Quant. Electron.*, vol. 47, no. 2, pp. 139–150, 2011.

[17] M. Gioannini, P. Bardella, and I. Montrosset, "Time-domain traveling-wave analysis of the multimode dynamics of quantum dot fabry-perot lasers," *IEEE J. Sel. Top. Quant. Electron.*, vol. 21, no. 6, pp. 1–11, 2015.

[18] L. L. Columbo, P. Bardella, I. Montrosset, and M. Gioannini, "Self-mode-locking in quantum dot unidirectional ring lasers: model and simulations," in *Numerical Simulation of Optoelectronic Devices (NUSOD), 2017 International Conference on*, 2017.

[19] E. Cabrera, O. G. Calderón, and J. M. Guerra, "Pattern formation in large-aspect-ratio single-mode inhomogeneously broadened lasers," *Phys. Rev. A*, vol. 70, p. 063808, Dec 2004.

[20] J. Mukherjee and J. G. McInerney, "Spatial mode dynamics in wide-aperture quantum-dot lasers," *Phys. Rev. A*, vol. 79, p. 053813, May 2009.

[21] J. Zehetner, C. Spielmann, and E. Krausz, "Passive mode locking of homogeneously and inhomogeneously broadened lasers," *Opt. Lett.*, vol. 17, no. 12, pp. 871–873, 1992.

[22] A. G. Vladimirov and D. Turaev, "New model for mode-locking in semiconductor lasers," *Radiophys. & Quant. Electron.*, vol. 47, no. 10-11, pp. 857–865, 2004.

[23] A. G. Vladimirov, D. Turaev, and G. Kozyreff, "Delay differential equations for mode-locked semiconductor lasers," *Opt. Lett.*, vol. 29, pp. 1221–1223, 2004.

[24] A. G. Vladimirov and D. Turaev, "Model for passive mode locking in semiconductor lasers," *Phys. Rev. A*, vol. 72, p. 033808, Sep 2005.

[25] M. Lichtner, "Spectral mapping theorem for linear hyperbolic systems," *Proc. Amer. Math. Soc.*, vol. 136, pp. 2091 – 2101, 2008.

[26] A. G. Vladimirov, A. S. Pimenov, and D. Rachinskii, "Numerical study of dynamical regimes in a monolithic passively mode-locked semiconductor laser," *Quantum Electronics, IEEE Journal of*, vol. 45, pp. 462–468, May 2009.

[27] A. Vladimirov, U. Bandelow, G. Fiol, D. Arsenijević, M. Kleinert, D. Bimberg, A. Pimenov, and D. Rachinskii, "Dynamical regimes in a monolithic passively mode-locked quantum dot laser," *J. Opt. Soc. B*, vol. 27, no. 10, pp. 2102–2109, 2010.

[28] E. Viktorov, P. Mandel, A.G.Vladimirov, and U. Bandelow, "A model for mode-locking in quantum dot lasers," *Appl. Phys. Lett.*, vol. 88, p. 201102 (3 pages), 2006.

[29] K. Engelborghs, T. Luzyanina, and G. Samaey, "DDE-BIFTOOL v.2.00: A MATLAB package for bifurcation analysis of delay differential equations," Tech. Rep. TW-330, K. U. Leuven, 2001.

[30] E. A. Avrutin and E. L. Portnoi, "Suppression of Q-switching instabilities in broadened-waveguide monolithic mode-locked laser diodes," *Opt Quant Electron*, vol. 40, pp. 655–664, 2008.

[31] C. Hönninger, R. Paschotta, F. Morier-Genoud, M. Moser, and U. Keller, "Q-switching stability limits of continuous-wave passive mode locking," *J. Opt. Soc. Am. B*, vol. 16, no. 1, pp. 46–56, 1999.